Electronic Supplementary Material (ESI) for RSC Advances.

Bicontinuous and cellular structures designing of PVDF membrane by using binary diluents for membrane distillation process

Ziyi Wang[a,d], Yuanyuan Tang[a]*, Baoan Li[b,c]*

[a] School of Environmental Science and Engineering, Southern University of Science and Technology, Shenzhen 518005, China

[b] Chemical Engineering Research Center, School of Chemical Engineering and Technology, Tianjin University, Tianjin 300354, China

[c] Collaborative Innovation Center of Chemical Science and Engineering (Tianjin), Tianjin 300354, China

[d] School of Chemical Engineering and Technology, Nankai University, Tianjin 300072, China

*Dr. Yuanyuan Tang, Assistant Professor, School of Environmental Science and Engineering, Southern University of Science and Technology, Shenzhen 518055, P. R. China, E-mail: tangyy@sustc.edu.cn

*Prof. Baoan Li, Chemical Engineering Research Center, School of Chemical Engineering and Technology, Tianjin University, Tianjin 300072, P. R. China, E-mail: baoan.li@gmail.com.

Including

Appendix 1. Calculation of porosity and pore size distribution

According to the gravimetric method, the membranes were immersed in the buffer tank filled with i-butanol (AR, Tianjin Jiangtian Chemical Technology Co. Ltd., China) for 24 h, and then taken out to be weighted immediately after removing i-butanol on the outer surface. The porosity of the fiber was calculated by the following equation [S1, S2]:

$$\varepsilon = \frac{m_1 - m_2}{\rho \Delta V} \qquad \text{Eq.(S1)}$$

Where m_1 is the weight of dry fibers, m_2 is the weight of wet fibers, ρ_1 is the density of PVDF and ρ_2 is the density of anhydrous alcohol.

In order to calculate the pore size, N_2 was forced to permeate from the inside to the outside of the hollow fibers. While the hollow fiber pores were wetted by a wetting solution (such as i-butanol, surface tension 23.0 dym/cm), the big pores with large diameters were burst firstly by the N_2 at low pressure. With increase of N_2 pressure the smaller pores were opened gradually. The smallest pores were penetrated finally at the highest pressure. The pore size distribution of membranes was calculated by Hagen-Poiseuille equation:

$$J = \frac{\pi d_i^4}{128 \eta \iota} \Delta P_i \qquad \text{Eq.(S2)}$$

Where J is volumetric flow rate, d_i is pore diameter, η is coefficient of viscosity (dynamic), l is length of pore and ΔP_i is pressure drop.

Actually, the measured pore flow rate at ΔP_i was the accumulative overall pore flow rate J_i which could be calculated from different overall pore size D_i. According to Eq.(S2), the increment of overall pore area S_i was calculated as below:

$$S_i = \frac{\pi}{4}(D_i^2 - D_{i-1}^2) = (8\pi\eta l)^{1/2}\left[\left(\frac{J_i}{\Delta P_i}\right)^{1/2} - \left(\frac{J_{i-1}}{\Delta P_{i-1}}\right)^{1/2}\right] \qquad \text{Eq.(S3)}$$

The pore diameter d_i was calculated according to Laplace equation:

$$d_i = 4\gamma \cos\theta / \Delta P_i \qquad \text{Eq.(S4)}$$

Where γ is the surface tension of the wetting solution, θ is the contact angle of wetting solution.

The pore number $N_{i-1,I}$ with the pore size ranging from d_{i-1} to d_i was obtained as:

$$N_{i-1,i} = \frac{S_i}{\frac{\pi}{4}\left(\frac{d_i + d_{i+2}}{2}\right)^2} \quad \text{Eq.(S5)}$$

The distribution of the pore size was determined by:

$$Frequency = \frac{N_{i-1,i}}{\sum_{i-1}^{m} N_{i-1,i}} \quad \text{Eq.(S6)}$$

Appendix 2: Figures of membrane fabrication and property measurements

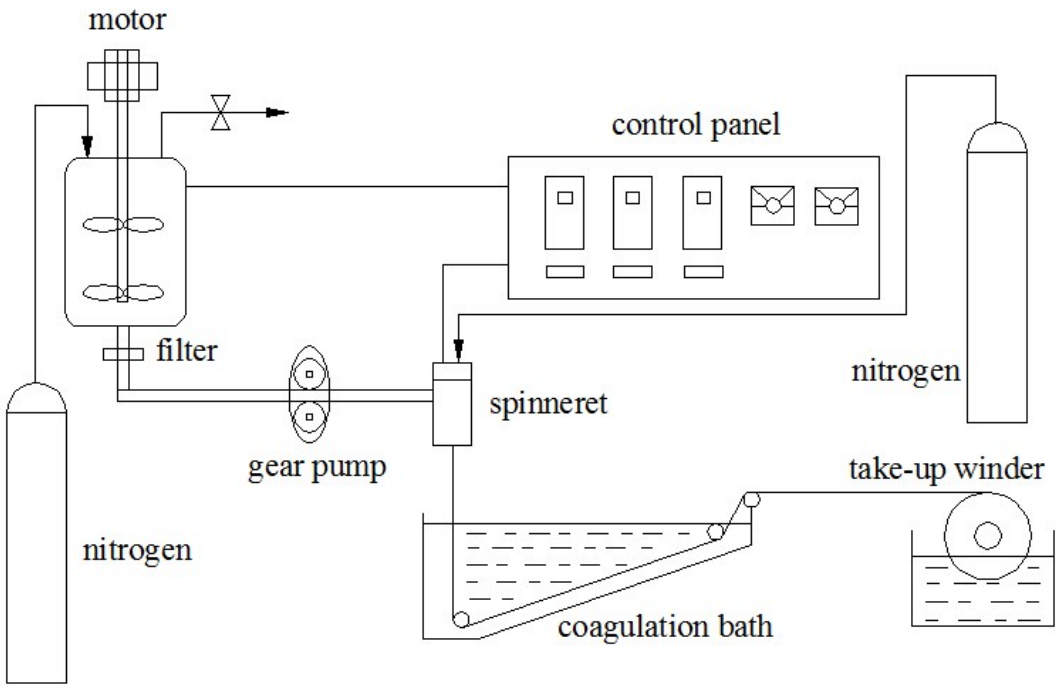

Fig.S1 Schematic diagram of the TIPS process for the preparation of the hollow fiber membranes

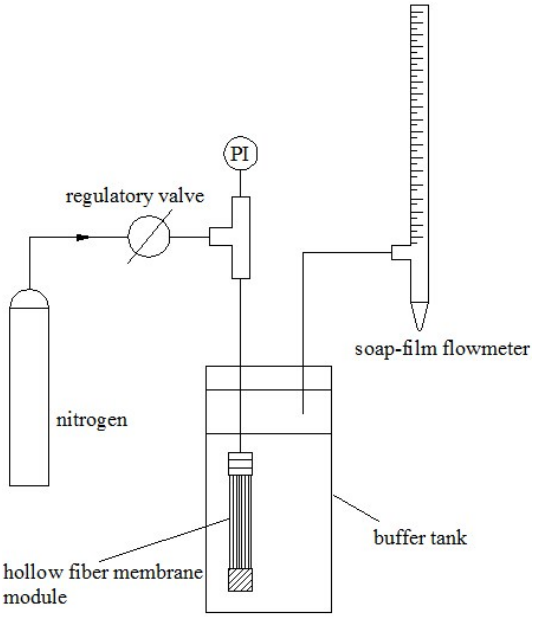

Fig.S2 Apparatus for measuring the porosity, mean pore size and pore size distribution of the fibers

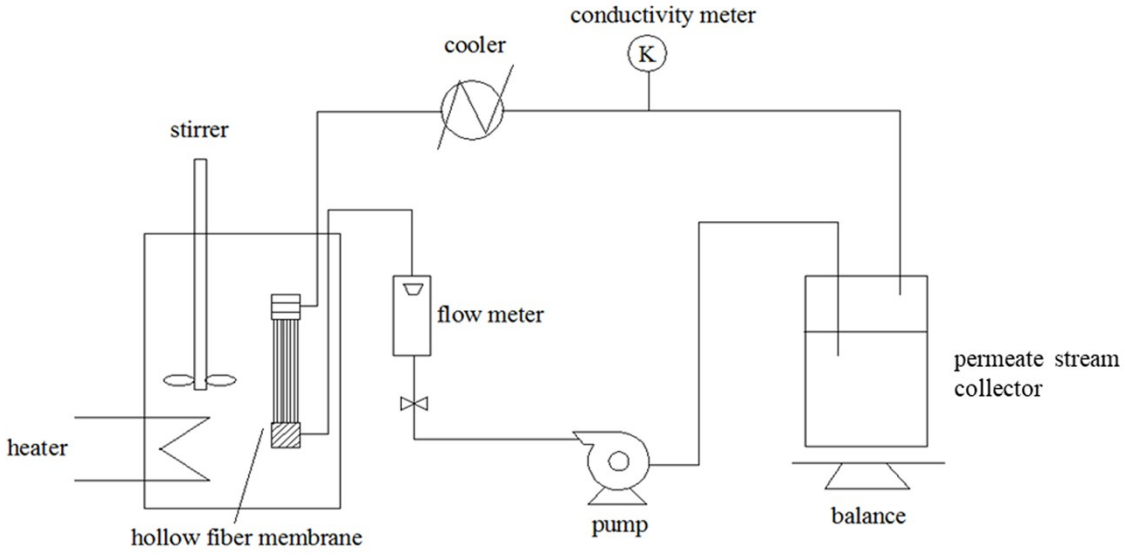

Fig.S3 Apparatus for measuring DCMD flux

Appendix 3: Phase diagram analysis

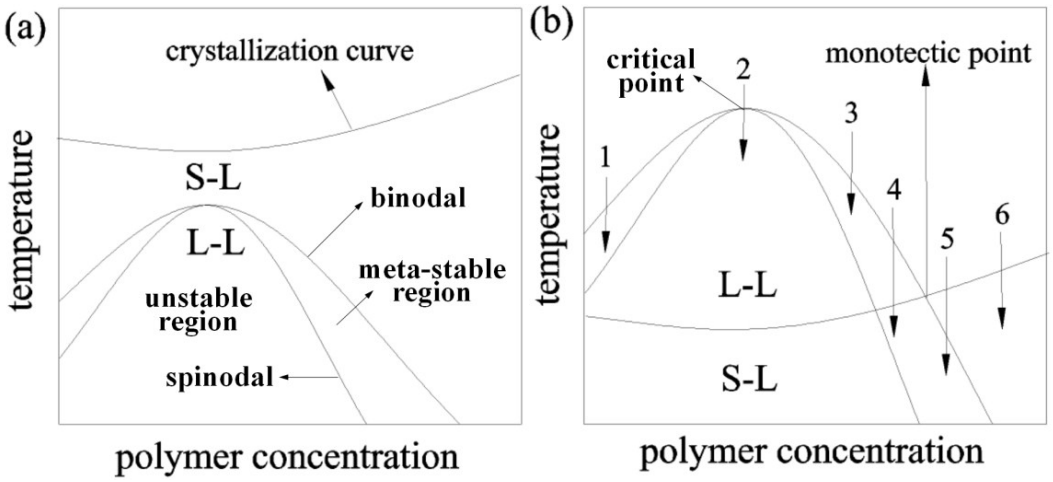

Fig.S4 Schematic phase diagram of casting solution in (a) strong polymer-diluent interaction and (b) weak polymer-diluent interaction

The TIPS process for all of the polymer-binary diluent systems can undergo in term of either solid-liquid (S-L) phase separation or liquid-liquid (L-L) phase separation. The major factor determining the occurrence of S-L or L-L phase separation is the compatibility of casting solution, which is quantified as the interaction parameter between polymer and diluent. For the casting solution in strong polymer-diluent interaction (Fig.S4a) [S3], S-L phase separation behavior has been observed predominantly, a representative spherulite structure is originated from a nucleation and growth mechanism. On occasion, the casting solution undergoes L-L phase separation subsequent to S-L phase separation when the temperature fells into the region of L-L phase separation which is very close to the crystallization line. The spherulite structure becomes fuzzy and indiscernible, with an eventual transition to cellular structure due to the influence of L-L phase separation. Otherwise, the discernable spherulitic, fibrous, or leafy structure can be qualitatively characterized in terms of S-L phase separation.

The casting solution undergoes L-L phase separation if there is a weak polymer-diluent interaction, the equilibrium phase diagram in Fig.S4b is used here to facilitate the explanation of dynamic membrane formation process [S3]. As the temperature decreases, the diminishing thermal energy weakens the interaction between polymer and diluent. The casting solution of initial composition separates into two phases in equilibrium with the same chemical potential but different density, a polymer-rich phase and a polymer-

lean phase. The critical point is defined as the point at which the binodal and the spinodal curves meet, indicating the critical temperature at which two phases can coexist is the mixture. The spinodal line divides the two-phase mixture into an unstable region below the spinodal curve, and a meta-stable region enclosed by the spinodal and binodal curves. The unstable and meta-stable terms refer to different resistance ability to the fluctuation of solution concentration. Phase separation mechanism (binodal or spinodal decomposition) and final morphology of the membrane are varied with the processing parameters such as quenching temperature, polymer concentration, as well as diluent composition.

When the system was quenched through the left branch of binodal curve as approach 1, there is no spontaneous phase separation in this meta-stable region of the phase diagram, since the system is stable to small concentration fluctuations. The polymer concentration is lower than the critical concentration, inducing the system becomes a dispersion of the polymer-rich phase droplets in a continuous polymer-lean phase droplets. As cooling continues to lower temperature, the polymer-rich phase droplets grow in size under the driving force of concentration gradient. A latex structure is produced as a result of the binodal phase separation. When the quench process was carried out as approach 2, the solution crosses the critical point and enters the unstable region directly. In this region, the phase separation can spontaneously take place where there is even a smallest concentration fluctuation, indicating the instability of the system in this composition range. According to the spinodal decomposition mechanism, the solution separates spontaneously into tiny bicontinuous polymer-lean and polymer-rich phase droplets. Subsequently, the polymer molecules and the diluent molecules in the two phases retract from each other driven by the minimization of the interfacial tension. After the phase separation, the cellular structure with closed macroviod is transformed from the combination of smaller pores. When the casting solution in certain composition follows the right branch of the binodal curve as approach 3, the region between the binodal and spinodal curves, a dispersion of polymer-lean phase droplets in a continuous polymer-rich phase droplets is transformed. The polymer-lean phase droplets grow constantly into bicontinuous structure at high volume fraction, and closed cellular structure at low volume fraction as temperature drops. Therefore, the spinodal phase separation is supposed to give rise to a highly bicontinuous structure. In the cooling scheme as approach 4, the casting solution undergoes L-L phase separation with subsequent polymer crystallization at high initial polymer concentrations. In this way, polymer crystallizes out of the polymer-rich phase droplets to form the spherulites and meanwhile the grown polymer-lean phase droplets are entrapped within the polymer spherulites when the temperature drops below the crystallization line under the L-L phase separation region. The collision of growing polymer-lean phase droplets produces the pores connecting the cells in the cellular structures, and the spherulites transform into cell walls eventually. As the casting solution cooling as approach 5, the essential polymer

crystallization into the spherulite structure, which is representative of crystallization by S-L phase separation, was performed upon the removal of thermal energy. However, the diluent is rejected from the growing spherulite and collects at the surface of each spherulite by the influence of ensuing L-L phase separation. With the continuous growth, the spherulites with more open surfaces or truncated spherulites with textured surfaces are yielded. The predominant structure generated from approach 6 is the spherulites structure which is only characterized in term of S-L phase separation. In conclusion, the final morphology of membrane can be schematically controlled by varying quenching rate, polymer concentration, as well as diluent composition.

Appendix 4. Morphology of membranes

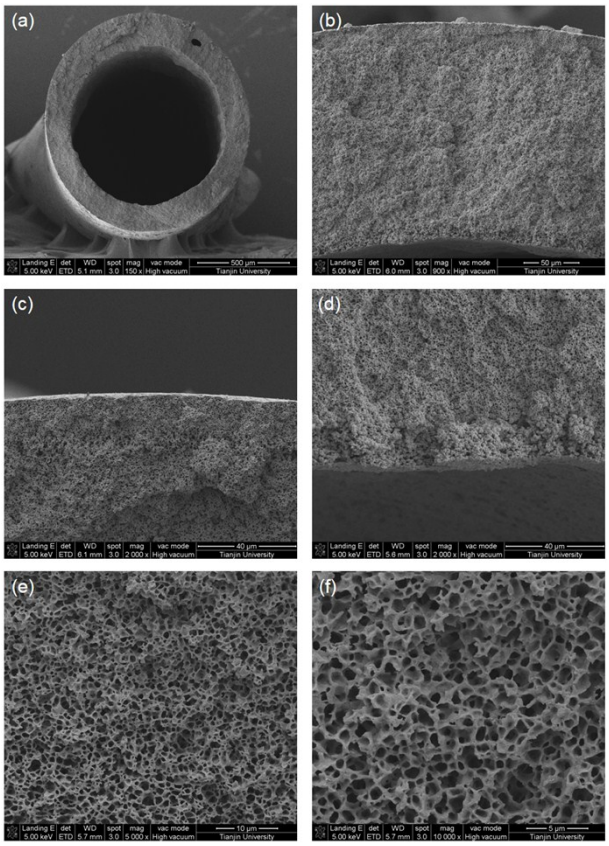

Fig.S5 The SEM images of the cross section: (a) the entire view, (b) the membrane wall, (c) the cross section near the outer surface, (d) the cross section near the inner surface, (e) the detailed view amplified by 5000 times, (f) the detailed view amplified by 10000 times

Reference:

[S1] ASTM C138. Standard Test Method for Unit Weight, Yield, and Air Content (Gravimetric) of Concrete, American Society of Testing and Materials, Philadelphia, PA, 1992.
[S2] S. Mochizuki, A.L. Zydney. Theoretical analysis of pore size distribution effects on membrane transport. Journal of Membrane Science, 1993, 82: 211-227.
[S3] D.R. Lloyd, S.S. Kim, K.E. Kinzer, Microporous membrane formation via thermally-induced phase separation. II. Liquid-liquid phase separation, J. Membr. Sci. 64 (1991) 1-11.